JOURNAL OF SOLID STATE CHEMISTRY **140,** 159–167 (1998)
ARTICLE NO. SC987725

Effect of Cation Arrangement on the Magnetic Properties of Lithium Ferrites ($LiFeO_2$) Prepared by Hydrothermal Reaction and Post-annealing Method

Mitsuharu Tabuchi,*,[1] Satoshi Tsutsui,† Christian Masquelier,‡ Ryoji Kanno,§ Kazuaki Ado,* Ichiro Matsubara,* Saburo Nasu,† and Hiroyuki Kageyama*

*Osaka National Research Institute, 1-8-31 Midorigaoka, Ikeda, Osaka 563, Japan; †Osaka University, 1-3 Machikaneyama-cho, Toyonaka, Osaka 560, Japan; ‡Laboratoire de Chimie des Solides, Université Paris XI Orsay, Batiment 414, 91405 Orsay Cedex, France; and §Kobe University, Rokkoudai-cho, Nada, Kobe, Hyogo 657, Japan

Received October 29, 1996; in revised form December 1, 1997; accepted December 2, 1997

The magnetic properties of several $LiFeO_2$ polymorphs (different cation arrangements in a cubic close-packed oxygen structure) have been examined by magnetic susceptibility measurements and Mössbauer spectroscopy. Samples with relatively low ferromagnetic impurity levels have been obtained by hydrothermal reaction of $FeCl_3 \cdot 6H_2O$ or FeOOH with $LiOH \cdot H_2O$ and subsequent annealing in air. α-$NaFeO_2$ with no detectable ferromagnetic impurity has been obtained by hydrothermal reaction of α-FeOOH and NaOH. While α-$NaFeO_2$ revealed only one anomaly at 11 K (Néel point) in the magnetic susceptibility–temperature curves, each $LiFeO_2$ sample shows two anomalies (40–50 and 90–280 K). Mössbauer data confirm that iron is present in the high-spin 3+ state according to the values of the internal field at 4.2 K and isomer shifts at 300 K. The relationship between the cation arrangements and the Néel temperature is discussed for $LiFeO_2$.

I. INTRODUCTION

Lithium transition metal oxides, $LiMO_2$ (M = V, Cr, Mn, Fe, Co, and Ni), have NaCl-type structures in which both M^{3+} and Li^+ occupy octahedral sites in a cubic close packing (ccp) of oxygen anions (1). The crystal structures may be divided into four main categories according to the cation arrangements within the ccp anion array.

(1) The α-$NaFeO_2$-type structure: this has alternating layers of trigonally distorted MO_6 and LiO_6 octahedra sharing edges. The unit cell is rhombohedral ($R\bar{3}m$). Many $LiMO_2$ (M = V, Cr, Co, and Ni) compounds have this structure. These materials are suitable for electrochemical lithium deintercalation–intercalation and have been examined as cathodes for lithium rechargeable batteries (2–6).

[1] To whom correspondence should be addressed.

(2) $LiMnO_2$-type structure (corrugated layered structure): this structure is a rock-salt-related structure with a distorted ccp oxygen anion array and alternating zigzag layers of Li^+ and Mn^{3+} cations. The unit cell is orthorhombic, space group *Pmnm*, closely related to that of γ-FeOOH.

(3) α-$LiFeO_2$-type structure: Li^+ and Fe^{3+} cations occupy randomly the octahedral sites. The unit cell is cubic, space group *Fm*3*m*.

(4) γ-$LiFeO_2$-type structure: Li^+ and Fe^{3+} order over the octahedral sites reducing the symmetry from cubic (*Fm*3*m*) to tetragonal ($I4_1/amd$), with a doubling of the cubic α-$LiFeO_2$-type cell. Li^+, Fe^{3+}, and O^{2-} occupy 4*a*, 4*b*, and 8*e* sites, respectively (7).

Figure 1 and Table 1 summarize the formation and crystal structures of $LiFeO_2$ polymorphs and α-$NaFeO_2$. Layered $LiFeO_2$ with the α-$NaFeO_2$ structure was obtained by Na^+/Li^+ ion exchange of α-$NaFeO_2$ in Li^+-containing molten salts at 250–400°C (8–10). Kanno *et al.* (11) synthesized a new polymorph of $LiFeO_2$ isostructural with $LiMnO_2$ (corrugated layered structure) by H^+/Li^+ ion exchange reaction from γ-FeOOH. The α and γ-$LiFeO_2$ polymorphs were prepared by a solid-state reaction–post-annealing method (12). Cation ordering commences on annealing α-$LiFeO_2$ in air at 300–500°C and proceeds to γ-$LiFeO_2$ through some intermediate, β phases (12–15). Two different crystal structures with monoclinic and tetragonal unit cells have been reported for the β polymorphs. Cation ordering was detected in the monoclinic phase, but not in the two tetragonal phases (12, 16). In this paper, the monoclinic phase is designated β′; the tetragonal phases β* and β″ have different c/a ratios. Previously, we prepared the α, β′, β″ and γ-polymorphs of $LiFeO_2$ by hydrothermal reaction of Fe^{3+} compounds (either α-FeOOH, $FeCl_3 \cdot 6H_2O$, $Fe(NO_3)_3 \cdot 9H_2O$, or $Fe_2(SO_4)_3 \cdot nH_2O$ (n = 6–9)) with a large excess of $LiOH \cdot H_2O$ at low temperatures (130–220°C), followed by post-annealing at 300–500°C (16).

0022-4596/98 $25.00

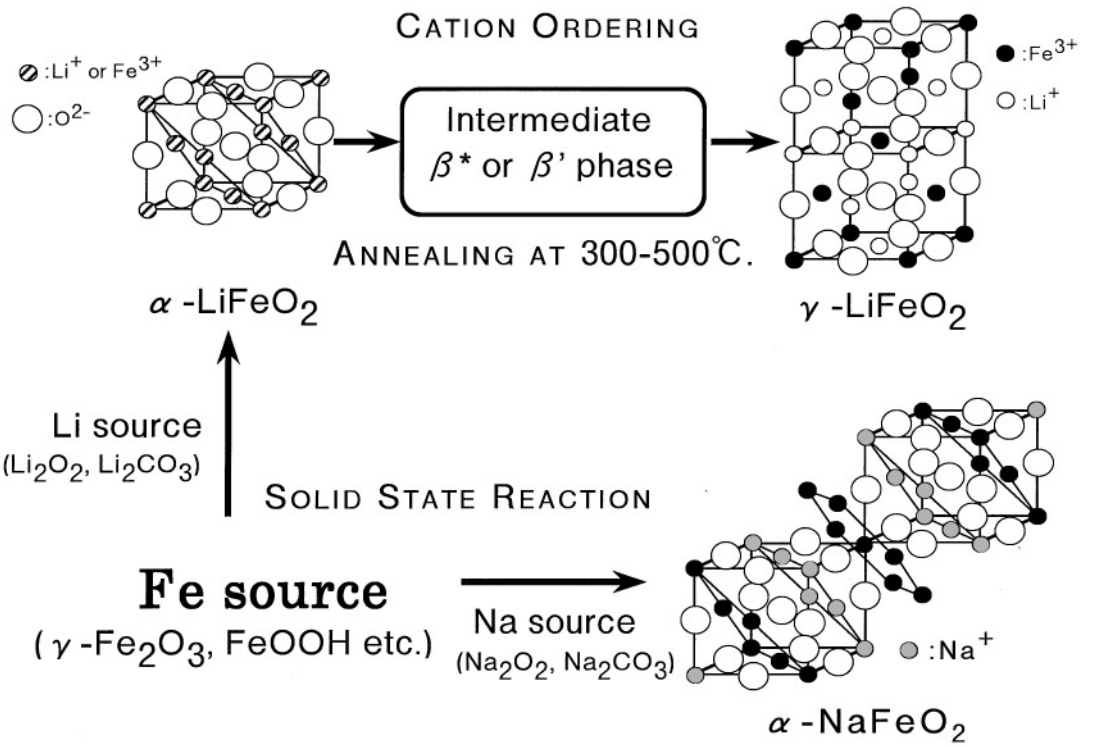

FIG. 1. Crystal structure and phase relationships for $LiFeO_2$ polymorphs and α-$NaFeO_2$.

α-$NaFeO_2$ was also obtained by hydrothermal reaction of α-FeOOH with concentrated NaOH aqueous solution at 130–150°C (19).

TABLE 1
Polymorphs of $LiFeO_2$

Phase	Crystal structure	Unit-cell parameter	Cation ordering	Reference
α'	Rock salt type (cubic, *Fm*3*m*)	$a = 4.158$ Å	ND[a]	12
β'	Monoclinic (*C*2/*c*)	$a = 8.571$ Å $b = 11.589$ Å $c = 5.147$ Å $\beta = 145.70°$	Present	13, 14
β''	Rock salt type (tetragonal)	$a = 4.152$ Å[b] $c = 4.192$ Å	ND[a]	16
β^*	Rock salt type (tetragonal)	$a = 4.09$ Å[b] $c = 4.28$ Å	ND[a]	12
γ	γ-$LiFeO_2$ type (tetragonal, $I4_1/amd$)	$a = 4.057$ Å $c = 8.759$ Å	Present	12
Layer	α-$NaFeO_2$ type (hexagonal, $R\bar{3}m$)	$a = 2.9632(7)$ Å $c = 14.636(4)$ Å	Present	10
Corrugated layer	$LiMnO_2$ type (orthorhombic, *Pnma*)	$a = 4.0610(5)$ Å $b = 2.9621(5)$ Å $c = 6.0319(11)$ Å	Present	11

[a] ND means that evidence of cation ordering could not be detected by powder X-ray diffraction measurement.

[b] The *a*-axis parameter was $\sqrt{2}$ times larger than the reported value for comparing directly with that of the α polymorph.

The existence of several polymorphs of $LiFeO_2$ allows the effect of cation arrangement on physical properties to be investigated. Fragmentary reports have appeared on the magnetic properties of α-, β^*-, and γ-$LiFeO_2$ as well as layered $LiFeO_2$ by magnetic susceptibility, neutron diffraction measurements, and Mössbauer spectroscopy (7, 10, 17). However, the presence of ferromagnetic β-$LiFe_5O_8$ impurity can markedly influence the magnetic properties. To elucidate the relationships between crystal structure and magnetic properties, a systematic study has been carried out using high-purity $LiFeO_2$ obtained by hydrothermal reaction. The effect of the Fe^{3+} ion arrangement on the magnetic properties is discussed by comparison with the magnetic data of α-$NaFeO_2$ prepared by the same method.

2. EXPERIMENTAL

α-FeOOH (reagent grade, Kanto Chemicals), $FeCl_3 \cdot 6H_2O$ (99% Wako Pure Chemicals), $LiOH \cdot H_2O$ (>98% Wako Pure Chemicals), and NaOH (>95% Ishizu Seiyaku) were used as starting materials.

To prepare the α polymorph, α-FeOOH was mixed with $LiOH \cdot H_2O$ (initial Li/Fe molar ratio = 30) in distilled water using a Teflon beaker to avoid reaction with the vessel. The mixture was treated hydrothermally at 220°C for 5 h using an autoclave (Sakashita Chemical Instruments). The products were washed repeatedly with distilled water to

eliminate residual $LiOH \cdot H_2O$ and dried at 100°C overnight. If the sample was heated at 160°C, the β'' phase, which has a slightly distorted α-$LiFeO_2$ structure, was obtained instead. γ-$LiFeO_2$ was obtained by annealing α-$LiFeO_2$ obtained hydrothermally at 480°C for 192 h in air.

To obtain the β^* polymorph, aqueous $FeCl_3 \cdot 6H_2O$ was poured over $LiOH \cdot H_2O$ in a Teflon beaker (initial Li/Fe ratio = 40), followed by hydrothermal treatment at 230°C for 48 h.

α-$NaFeO_2$ was obtained by hydrothermal treatment of a mixture of α-FeOOH (30 g) and concentrated NaOH aqueous solution (60 mol/kg of H_2O) at 220°C for 7 h. Products were washed with ethanol to avoid decomposition in water.

The samples were identified by X-ray diffraction (XRD, Cu$K\alpha$ radiation, Rigaku Rotaflex/RINT). Si and W powders were used as internal standards for refinement of lattice parameters.

Particle sizes and shapes were observed by transmission electron microscopy (TEM, H-300 Hitachi). Li contents and Na/Fe ratios were determined by atomic absorption and ICP emission spectroscopy, respectively.

Magnetization and magnetic susceptibility were measured between 83 and 300 K and between 1.8 and 12.5 kOe with a magnetic balance using the Farady method (MB-3, Shimadzu). Since small spontaneous magnetizations (M_s) were observed in magnetization–magnetic field (M–H) curves at both 83 and 300 K, the contribution of M_s to the total magnetization value at each magnetic field between 1.8 and 12.5 kOe was subtracted to obtain the magnetic susceptibility values. Temperature and magnetic susceptibility data were calibrated using $(NH_4)_2Mn(SO_4)_2 \cdot 6H_2O$ as the standard. A SQUID magnetometer (MPMS2, Quantum Design) was used to measure the magnetization between 5 and 300 K.

^{57}Fe Mössbauer spectra were measured at three temperatures (300, 77, and 4.2 K). α-Fe was used as standard. Velocity calibration was performed using data of α-Fe at 300 K.

3. RESULTS AND DISCUSSION

3.1. Hydrothermal Preparation and Magnetic Properties of α-$NaFeO_2$

All XRD peaks of α-$NaFeO_2$ observed in the powder diffraction pattern for this sample could be indexed on a hexagonal cell ($R\bar{3}m$ (18), $a = 3.02517(8)$ Å, $c = 16.0916(6)$ Å). No impurity phases were detected by XRD. The Na/Fe ratio was 1.05(1) by ICP emission spectroscopy, indicating that the sample was essentially stoichiometric. No spontaneous magnetization originating from ferromagnetic impurities was observed down to 5 K (Figs. 2a and 3). The effective magnetic moment (μ_{eff}), and Weiss temperature (θ) values were calculated to be 5.55(1) μ_B) and +7(1) K by fitting the χ_m^{-1}–T plots with the Curie–Weiss law ($\chi_m^{-1} = (T - \theta)/C_m$, where C_m is the Curie constant) between 83 and 290 K (Fig. 2b). The μ_{eff} value was close to a spin-only value of high-spin Fe^{3+} (5.92 μ_B) and that reported by Ichida (5.8 μ_B) (19). The isomer shift (+0.37 mm/s) obtained by Mössbauer spectroscopy at 300 K is typical of high-spin Fe^{3+}. The magnetic data shown in Figs. 2a and 3 are consistent with a stoichiometric sample, supporting the results from the XRD and chemical analysis data. The positive θ value suggests that ferromagnetic interactions are present in α-$NaFeO_2$. Although the Néel temperature (11 K, Fig. 3) is similar to that of Ichida's sample (11 ± 1 K (19)), the θ value (+7 K) is of opposite sign to that of Ichida (−10 K). Our preliminary results indicate that α-$NaFeO_2$ decomposed to γ-Fe_2O_3 and/or Fe_3O_4 in the presence of water. Both of these iron oxides have a ccp oxygen array similar to that of α-$NaFeO_2$ and could act as ferromagnetic impurities. Therefore, that μ_{eff} and θ values were plotted against the spontaneous magnetization (M_s) at 300 K (Fig. 4). While the positive θ (>4 K) and μ_{eff} values below 5.7 μ_B were obtained at low spontaneous magnetization below 0.02 Gcm^3/g, negative θ and μ_{eff} values above 5.9 μ_B were obtained at high spontaneous magnetization above 0.08 $G\,cm^3/g$. The difference in θ and μ_{eff} values between the present and previous data (19) may

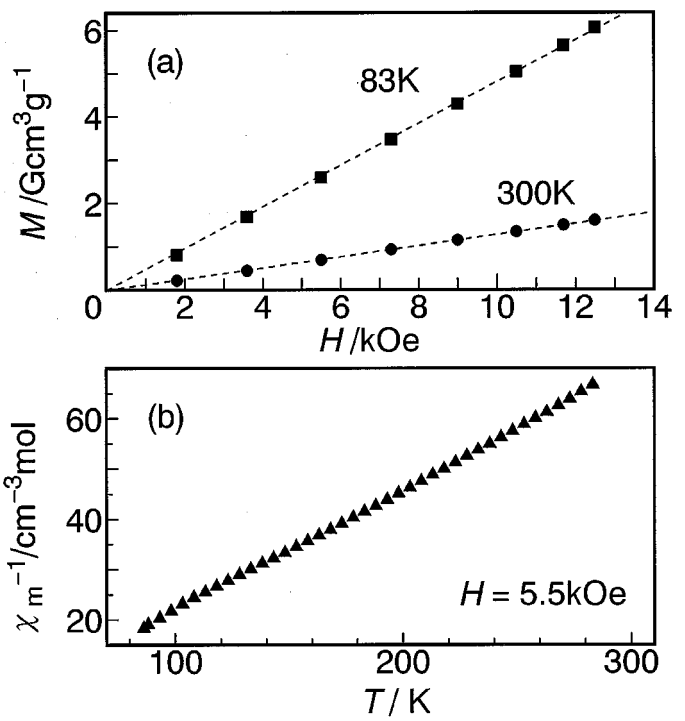

FIG. 2. Field dependence of magnetization at 83 and 300 K (a) and the temperature dependence of the inverse molar susceptibility between 83 and 290 K for α-$NaFeO_2$ prepared by hydrothermal reaction of a mixture of α-FeOOH and NaOH at 220°C for 7 h (b).

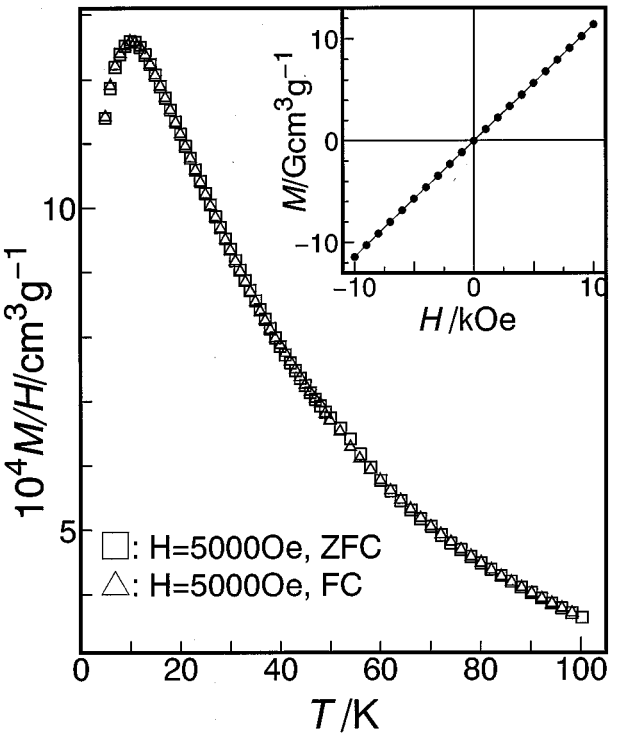

FIG. 3. Temperature dependence of the normalized magnetization by magnetic field for α-$NaFeO_2$ between 5 and 100 K at 5 kOe. FC and ZFC denote field cooling and zero field cooling runs, respectively. Field dependence of magnetization at 5 K is shown as the inserted figure.

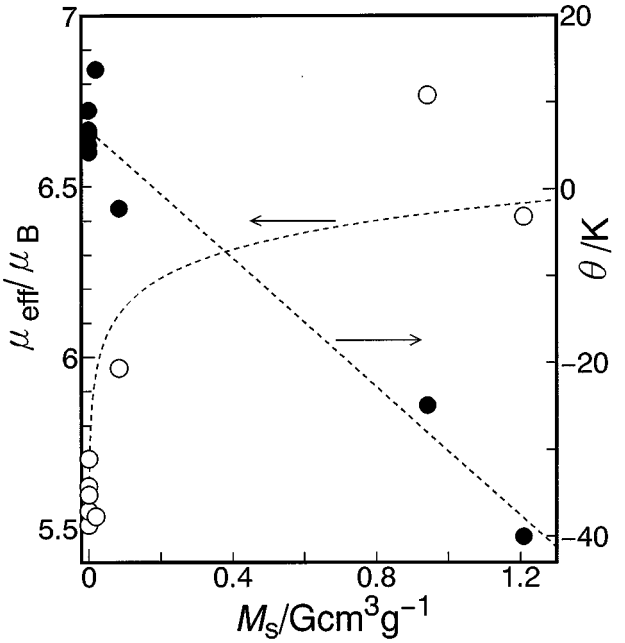

FIG. 4. Relationship between the effective magnetic moment (μ_{eff}), the Weiss temperature (θ), and the spontaneous magnetization (M_s) at 300 K for hydrothermally obtained α-$NaFeO_2$ samples. A broken curve and a straight line indicate the trend in the M_s–μ_{eff} plots and the M_s–θ plots, respectively.

be attributed to the difference in the content of ferromagnetic impurity. This observation is also consistent with the proposed antiferromagnetically ordered structure containing ferromagnetically ordered (104) planes below 11 K (Néel temperature) (20).

3.2. *Phase Purity of $LiFeO_2$ Polymorphs*

Four $LiFeO_2$ samples (α, β'', β* and γ polymorphs) were characterized by magnetic susceptibility measurements and Mössbauer spectroscopy. The monoclinic β' sample was not measured because it contained a small amount of α-$LiFeO_2$. The ratio of observed to calculated Li contents by atomic absorption spectroscopy, assuming the stoichiometric ($LiFeO_2$) composition, is 0.96–0.99, indicating that the composition of each sample is nearly stoichiometric. Although each sample was single phase by XRD, some ferromagnetic impurities below the XRD detection level can affect magnetic susceptibility data. Indeed, if a sample contains 1 wt% of β-$LiFe_5O_8$ as ferromagnetic impurity ($M_s = 65$ G cm^3/g, $T_c = 943$ K (21)), the observed magnetization value (ca. 0.65 G cm^3/g) is sufficient to significantly change the bulk magnetic data for $LiFeO_2$ (see Fig. 5), as will be described later.

3.3. *Formation of an Intermediate β*-$LiFeO_2$ Polymorph*

Two possible structures of β polymorphs have been proposed by Anderson and Schieber (12) for the tetragonal β* phase and by Famery *et al.* (15) and Brunel and Bergevin (13) for the monoclinic β' variant (see Table 1). We also observed two intermediate phases during cation ordering from the α to the γ phase (16). The monoclinic phase formed micron-sized α-$LiFeO_2$ powder consisting of about 1-μm particles on post-annealing, whereas the tetragonal phase was obtained by firing a mixture of submicron powders of the α and β* polymorphs (16). Neither β*-$LiFeO_2$ nor β'-$LiFeO_2$ was isolated by hydrothermal treatment and post-annealing (16). However, the β*-$LiFeO_2$ phase was obtained as a single phase using prolonged hydrothermal treatment at nearly the same temperature (220–230°C) during the transformation from α to γ (Table 2). Such behavior is consistent with Barriga's results (22), in which the crystal structure depends markedly on the time for hydrothermal reaction. Moreover, a difference in particle size between the β* and γ polymorphs was detected by TEM. The particle size (β* polymorph) after short reaction time (48 h) is less than 0.1 μm, whereas the particle size of the γ polymorph after prolonged hydrothermal treatment (168h) reached 0.3 μm. The monoclinic distortion and cation ordering of the β' phase may be suppressed by decreasing the particle size of the starting $LiFeO_2$ powder. The reported tetragonal β'' phase (16) ($a = 8.155$ Å, $c = 8.627$ Å) is apparently a

TABLE 2
Effect of Hydrothermal Conditions on Products of the $FeCl_3 \cdot 6H_2O$–$LiOH \cdot H_2O$ Reaction (Li/Fe = 40)

Hydrothermal condition	Products Main phase (minor phase)
230°C, 3 h	α-$LiFeO_2$ (β-$LiFe_5O_8$)
220°C, 5 h	α-$LiFeO_2$ (β*-$LiFeO_2$)
230°C, 24 h	β*-$LiFeO_2$ (α-$LiFeO_2$)
230°C, 48 h	β*-$LiFeO_2$
230°C, 72 h	β*-$LiFeO_2$ (γ-$LiFeO_2$)
230°C, 168 h	γ-$LiFeO_2$

mixture of β*-$LiFeO_2$ and β-$LiFe_5O_8$, by comparison of the XRD pattern with that of the β* phase.

3.4. Magnetic Properties of $LiFeO_2$

We checked the quality of our samples first by the field dependence of the magnetization at 295 K (Fig. 5). The spontaneous magnetization was less than 0.10 G cm^3/g for all $LiFeO_2$ samples, indicating that the β-$LiFe_5O_8$ content was less than 0.15 wt%, assuming that the ferromagnetic impurity is only $LiFe_5O_8$. These contents are significantly lower than those given previously (0.8–0.9 wt%) (17).

The temperature dependence of the inverse molar susceptibilities was linear above 240 K for α- and β″-$LiFeO_2$ (Fig. 6a). Deviation from Curie–Weiss paramagnetic behavior was observed below 300 K for the β* polymorph due to the presence of an anomaly around 140 K. The calculated μ_{eff} and θ values were 4.53(3) μ_B and −186(3) K for α-$LiFeO_2$ and 4.80(2) μ_B and −228(3) K for β″-$LiFeO_2$,

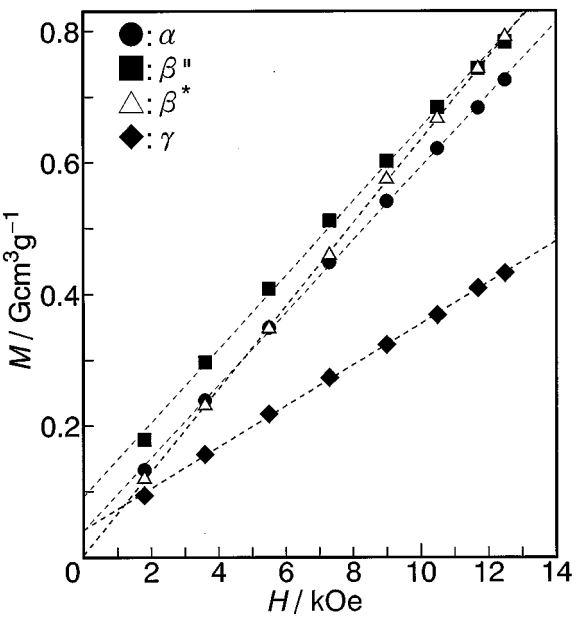

FIG. 5. Magnetic field dependence of the magnetization for hydrothermally obtained $LiFeO_2$ samples at 295 K.

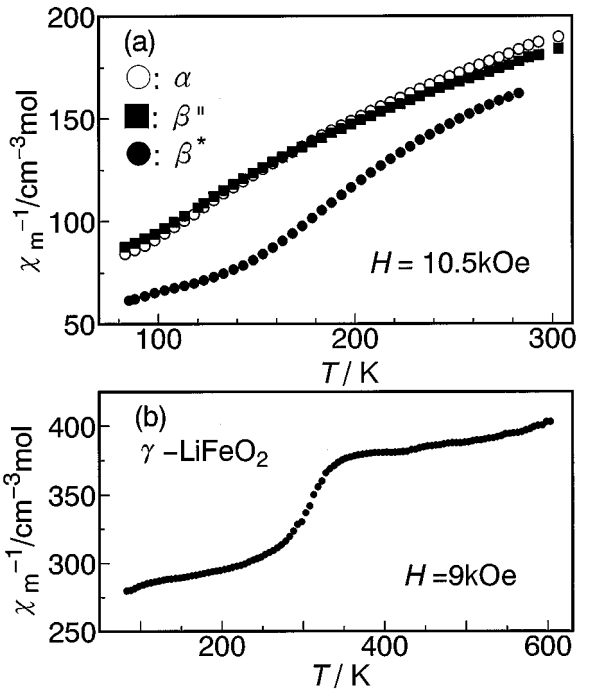

FIG. 6. Temperature dependence of the inverse molar suceptibility for hydrothermally obtained $LiFeO_2$ (α, β″, and β* polymorphs) between 83 and 300 K (a) and for γ-$LiFeO_2$ between 83 and 600 K (b).

assuming that the Curie–Weiss law could apply to the data above 240 K. Their negative θ values are consistent with the antiferromagnetic behavior below room temperature (see Fig. 8); previous data gave $\theta = -400$ K for α-$LiFeO_2$ (17). However, the observed μ_{eff} values are smaller than the spin-only value of high-spin Fe^{3+} (5.92 μ_B) and previous data (5.91 μ_B for α, 5.48 μ_B for β*). To clarify the difference between the present and previous data, μ_{eff} is plotted against M_s at 295 K for α-$LiFeO_2$ samples with various amounts of ferromagnetic impurity in Fig. 7. The μ_{eff} value reached the spin-only of high spin Fe^{3+} with increasing M_s value. Therefore, the relatively high μ_{eff} value of the previous α-$LiFeO_2$ sample (17) is attributed to the presence of a ferromagnetic impurity such as β-$LiFe_5O_8$. Similar low μ_{eff} values have been observed in the perovskites Ba_2FeNbO_6 (3.5 μ_B) and Sr_2FeTaO_6 (3.3 μ_B) in which high-spin Fe^{3+} cations partially occupied the *B* sites (23). In this structure, disordered Fe^{3+} and Nb^{5+} form a simple cubic sublattice, similar to the face-centered cubic lattice consisting of Li^+ and Fe^{3+} cations in α-$LiFeO_2$.

The χ_m^{-1} vs. *T* plots for γ-$LiFeO_2$ (Fig. 6b) above 83 K revealed an anomaly around 300 K associated with the Néel temperature. The data above 350 K do not fit the Curie–Weiss law, because unacceptable μ_{eff} and θ values (7.4 μ_B and −3000 K) were obtained. The Curie–Weiss paramagnetism observed previously above 350 K (μ_{eff} = 5.94 (17) and 5.6 μ_B (7)) may be caused by the presence of a ferromagnetic impurity such as $LiFe_5O_8$, because

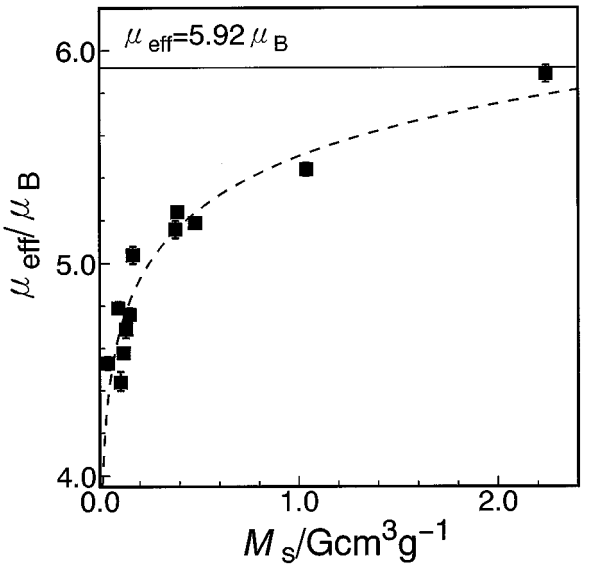

FIG. 7. Relationship between effective magnetic moment (μ_{eff}) and spontaneous magnetization (M_s) at 295 K for hydrothermally obtained α-$LiFeO_2$. The $\mu_{eff} = 5.92\ \mu_B$ line corresponds to the value expected for the spin-only contribution of high-spin Fe^{3+}. The broken curve indicates the trend in the data.

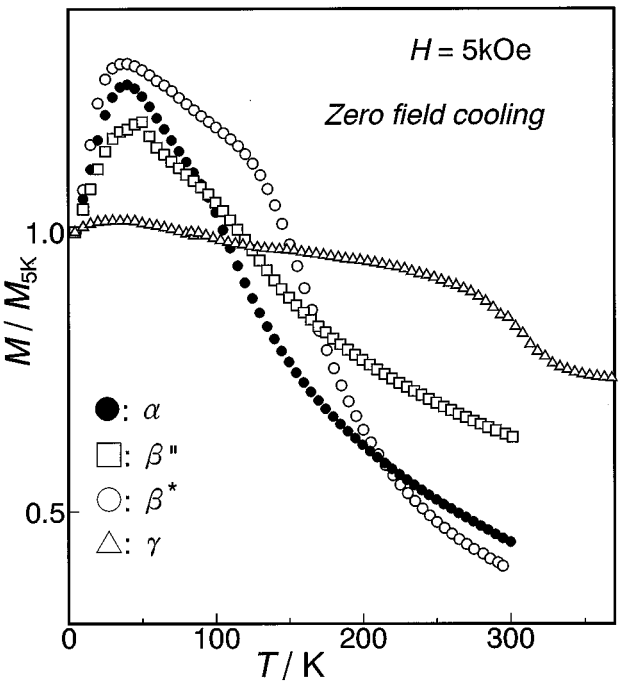

FIG. 8. Temperature dependence of magnetization normalized by the data at 5 K (M/M_{5K}) or hydrothermally obtained $LiFeO_2$ (α, β'', β^*, and γ polymorphs).

the impurity content of our sample (0.08 wt%) is much smaller than that of the previous data (17) (0.8 wt%).

The shape of the temperature dependence of magnetization normalized to that at 5 K (M/M_{5K}–T curves, Fig. 8) is similar for $LiFeO_2$ samples. Maxima were observed around 50 K with anomaly points above 90 K, indicating antiferromagnetic behavior for all $LiFeO_2$ samples: these additional anomalies occurred at 90(5) K for α, 100(5) K for β'', 140(5) K for β^*, and 280(5) K for γ. The temperature of the anomalies seemed to increase with cation ordering in the sequence $\alpha \rightarrow \beta^* \rightarrow \gamma$. The anomalies at 40(5) and 280(5) K for the α and γ phases agree with previous results (7, 17). However, the Néel temperature is still unknown due to the presence of two anomalies for each data set.

Mössbauer spectroscopy data were collected at 300, 77,and 4.2 K. A doublet was observed for each sample except for γ-$LiFeO_2$ at 300 K (Fig. 9), which indicates a paramagnetic state. The γ polymorph showed coexistence of a broad component and a doublet, which is characteristic of proximity to the Néel temperature (315 K (7), 280(5) K from Fig. 8). The isomer shift values listed in Table 3 are similar for all samples (+0.36–0.40 mm/s) and are typical of high-spin Fe^{3+} compounds, in agreement with previous data; +0.38 mm/s for γ-$LiFeO_2$ and +0.35 mm/s for α-$LiFeO_2$ (7).

Spectra at 4.2 K (Fig. 10) for all $LiFeO_2$ samples reveals sextets indicating a magnetic ordered state. However, the sextets except for that of γ-$LiFeO_2$ show asymmetric broadening. Each spectrum was fitted by superimposing two sets of sextets with slightly different isomer shifts and internal fields (H_{int}). The internal fields (47–52 T, Table 3) were typical of high-spin Fe^{3+}. The appearance of two sextets means that two different magnetic interactions must be considered, indicating the presence of two different environments around the Fe^{3+} ions. The fraction of the component with higher internal field increased and the peak width of each sextet became narrower in the sequence $\alpha \rightarrow \beta^* \rightarrow \gamma$, indicating that disordering of Fe^{3+} probably led to a lowering of internal field values and broadening of the sextets. The presence of two types of magnetic contributions from normalized magnetization and Mössbauer data is probably due to incomplete ordering of Fe^{3+} in the γ polymorph, probably originating from the low annealing temperature, below 480°C. Complete ordering should result in a symmetrical sextet originating from only one crystallographic site of iron (4*a* site in the space group $I4_1/amd$).

All Mössbauer spectra at 77 K (Fig. 11) indicate magnetic ordering; therefore the anomalies above 90 K on the M/M_{5K}–T curves must correspond to the Néel temperatures (T_N).

Mössbauer data show iron to be present as high-spin Fe^{3+} for all $LiFeO_2$ samples, like that of α-$NaFeO_2$. Thus, no variation in valence state of iron was detected by either magnetic susceptibility or Mössbauer measurements. However, the large difference in Néel temperature for α-$NaFeO_2$ and $LiFeO_2$ could be related to the Fe^{3+} arrangement on octahedral sites in a ccp oxygen array. The suppression of magnetic order in α-$NaFeO_2$ may originate from the two-

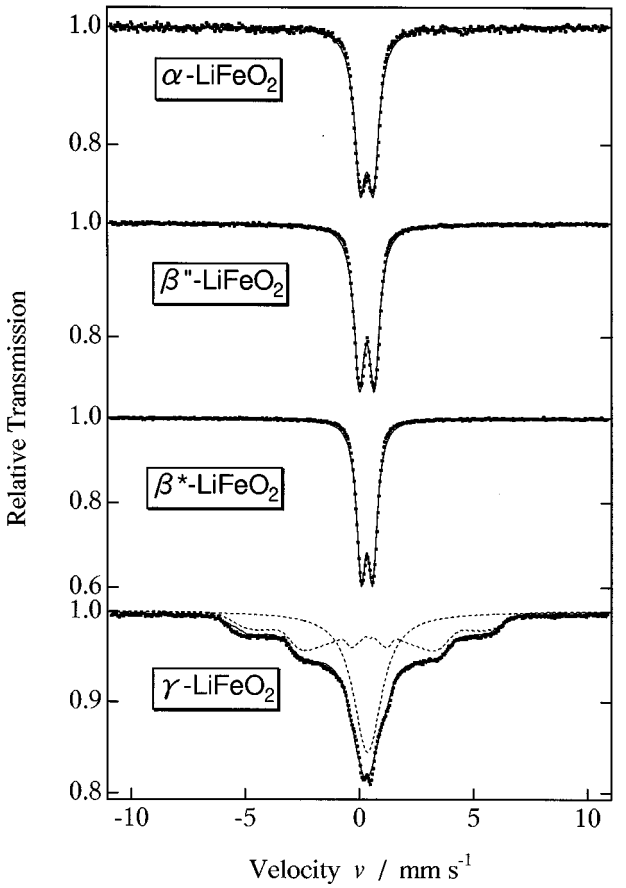

FIG. 9. ^{57}Fe Mössbauer spectra at 300 K for hydrothermally obtained $LiFeO_2$. Broken curves for the γ polymorph are fits to the observed spectrum.

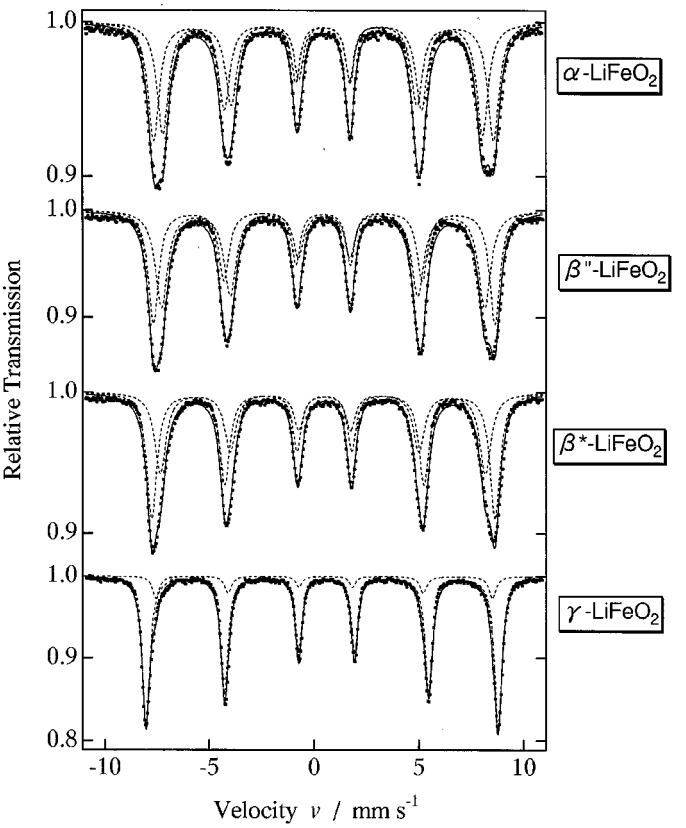

FIG. 10. ^{57}Fe Mössbauer spectra at 4.2 K for hydrothermally obtained $LiFeO_2$. Broken curves represent the sextet of each component fitted to the observed spectrum.

dimensional arrangement of Fe^{3+} ions (see Fig. 1), leading to strong Fe^{3+}–O^{2}–Fe^{3+} 180° interaction (24) between neighboring Fe^{3+} layers. The layered $LiFeO_2$ exhibited antiferromagnetism with a Néel temperature of 20 K (10), similar to that (11 K) of α-$NaFeO_2$. In $LiNiO_2$ with the α-$NaFeO_2$ structure, a sample close to ideal ordered cation arrangement exhibited a low magnetic transition temperature, below 10 K, whereas a slightly cation-disordered sample had a magnetic transition temperature above 50 K (25–27). Consequently, the presence of additional anomaly points (Néel temperature) above 90 K (Fig. 8) for our $LiFeO_2$ samples may be related to the deviation in the Fe^{3+}

TABLE 3
Mössbauer Parameters of the $LiFeO_2$ Samples Measured at 300 and 4.2 K

	300 K			4.2 K				
Samples	IS (mm s^{-1})	QS (mm s^{-1})	Γ (mm s^{-1})	IS (mm s^{-1})	QS (mm s^{-1})	Γ (mm s^{-1})	H_{int} (T)	Area ratio (%)
α-$LiFeO_2$	+0.37	0.58	0.60	+0.49	+0.026	0.65	50	51.1
				+0.50	−0.078	0.66	47	48.9
β″-$LiFeO_2$	+0.36	0.66	0.55	+0.50	+0.040	0.60	51	46.6
				+0.50	−0.055	0.71	48	53.4
β*-$LiFeO_2$	+0.36	0.51	0.48	+0.50	−0.055	0.58	51	57.8
				+0.50	−0.093	0.66	48	42.2
γ-$LiFeO_2$	+0.40[a]	0.23	1.44	+0.51	−0.22	0.43	52	88.0
				+0.53	−0.081	0.39	50	12.0

[a] Unresolved components ($H_{max} \approx 44$ T) are also presented in this spectrum, because the measuring temperature was close to the Néel temperature.

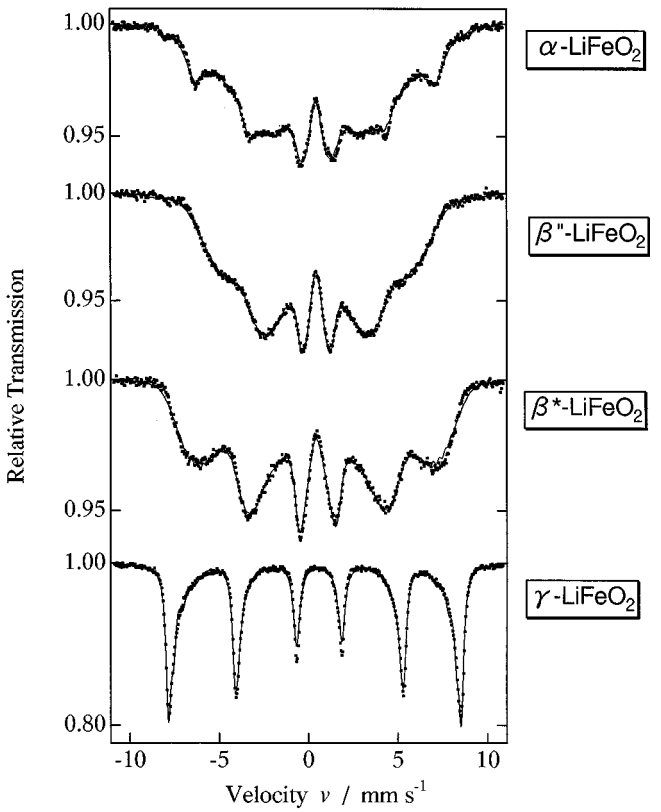

FIG. 11. ^{57}Fe Mössbauer spectra at 77 K for the hydrothermally obtained $LiFeO_2$.

arrangement from the α-$NaFeO_2$-type structure. However, the difference in the Néel temperature between our $LiFeO_2$ samples has still not been explained.

β''-, β^*-, and γ-$LiFeO_2$ have tetragonally distorted, α-$LiFeO_2$-type unit cells. The degree of tetragonal distortion was estimated from the c/a ratio of unit cell parameters for the α, β'', and β^* polymorphs and from the $c/2a$ ratio for the γ polymorph with values of 1.00 for α, 1.01 for β'', 1.05 for β^*, and 1.08 for γ. Thus the increase in tetragonality appears to be associated with cation ordering. Also, the magnetic transition temperature increased with the degree of tetragonal distortion from cubic α-$LiFeO_2$ to tetragonal γ-$LiFeO_2$ (Fig. 12). Therefore, the relatively high Néel temperature of γ-$LiFeO_2$ could be associated with the cation ordering accompanying the increase in tetragonal distortion.

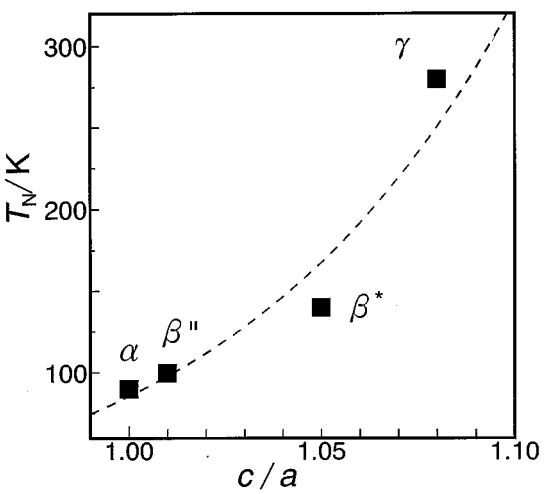

FIG. 12. Néel temperature (T_N) as a function of the tetragonality (the c/a ratio) for hydrothermally obtained $LiFeO_2$. A $c/2a$ value was used for the γ polymorph due to the presence of a superstructure along the c-axis. The broken curve indicates the trend of the plotted data.

4. CONCLUSIONS

Magnetic properties of lithium ferrites and a sodium ferrite prepared by a hydrothermal–post annealing method were examined to investigate crystal structure–magnetic behavior relationships. Using hydrothermal reaction, we obtained samples with a satisfactorily low (<0.15 wt%) ferromagnetic impurity level. The effective magnetic moments and Weiss temperatures for α-$NaFeO_2$ and α-$LiFeO_2$ were affected markedly by the spontaneous magnetization originating from ferromagnetic impurities. Thus, a ferromagnetic impurity gave an anomalously high effective magnetic moment for α-$LiFeO_2$ and α-$NaFeO_2$ and a negative Weiss temperature for α-$NaFeO_2$. The observed μ_{eff} value for α-$LiFeO_2$ with low impurity level is lower than the spin-only value of high-spin Fe^{3+}, as found for Ba_2FeNbO_6 and Sr_2FeTaO_6 with the cubic perovskite structure in which high-spin Fe^{3+} ions partially occupy the B sites. The Mössbauer spectra at 300 and 4.2 K for all $LiFeO_2$ samples confirmed that the iron is in the 3+ high-spin state. The temperature dependence of the normalized magnetization reveals antiferromagnetic order below 300 K for all samples. While α-$NaFeO_2$ was a simple antiferromagnet below 11 K, $LiFeO_2$ samples had two anomalies, at 40–50 and 90–280 K. The anomalies above 90 K are confirmed as Néel points by Mössbauer measurements. The magnetic transition temperatures of the α-, β^*-, β''-, and γ-$LiFeO_2$ samples are governed by the degree of cation ordering and/or the tetragonal distortion.

ACKNOWLEDGMENTS

We thank Dr. Y. Takeda (Mie University) for fruitful discussions and performing ICP measurements. We express our gratitude to Prof. A. R. West (University of Aberdeen) for fruitful discussions.

REFERENCES

1. T. A. Hewston and B. L. Chamberland, *J. Phys. Chem. Solids* **48,** 97 (1987).
2. R. J. Gummow and M. M. Thackeray, *Mater. Res. Bull.* **27,** 327 (1992).
3. J. R. Dahn, U. von Sacken, M. W. Juzkow, and H. Al-Janaby, *J. Electrochem. Soc.* **138,** 2207 (1991).

4. C. D. W. Jones, E. Rossen, and J. R. Dahn, *Solid State Ionics* **68,** 65 (1994).
5. J. N. Reimers, E. Rossen, C. D. Jones, and J. R. Dahn, *Solid State Ionics* **61,** 335 (1993).
6. J. N. Reimers, E. W. Fuller, E. Rossen, and J. R. Dahn, *J. Electrochem. Soc.* **140,** 3396 (1993).
7. D. E. Cox, G. Shirane, P. A. Flinn, S. L. Ruby, and W. J. Takei, *Phys. Rev.* **132,** 1547 (1963).
8. V. B. Nalbandyan and I. L. Shukaev, *Russ. J. Inorg. Chem.* **32,** 453 (1987).
9. B. Fuchs and S. Kemmer-Sack, *Solid State Ionics* **68,** 279 (1994).
10. T. Shirane, R. Kanno, Y. Kawamoto, Y. Takeda, M. Takano, T. Kamiyama, and F. Izumi, *Solid State Ionics* **79,** 227 (1995).
11. R. Kanno, T. Shirane, Y. Kawamoto, Y. Takeda, M. Takano, M. Ohashi, and Y. Yamaguchi, *J. Electrochem. Soc.* **143,** 2435 (1996).
12. J. C. Anderson and M. Schieber, *J. Phys. Chem. Solids* **25,** 961 (1964).
13. M. Brunel and F. D. Bergevin, *J. Phys. Chem. Solids* **29,** 163 (1968).
14. R. Famery, P. Bassoul, and F. Queyroux, *J. Solid State Chem.* **57,** 178 (1985).
15. R. Famery, P. Bassoul, and F. Queyroux, *J. Solid State Chem.* **61,** 293 (1986).
16. M. Tabuchi, K. Ado, H. Sakaebe, C. Masquelier, H. Kageyama, and O. Nakamura, *Solid State Ionics* **79,** 220 (1995).
17. J. C. Anderson, S. K. Dey, and V. Halpern, *J. Phys. Chem. Solids* **26,** 1555 (1965).
18. Y. Takeda, K. Nakahara, M. Nishijima, N. Imanishi, and O. Yamamoto, *Mater. Res. Bull.* **29,** 659 (1994).
19. T. Ichida, T. Shinjo, Y. Bando, and T. Takada, *J. Phys. Soc. Jpn.* **29,** 795 (1970).
20. Z. Tomokovicz and B. V. Laar, *Phys. Status. Solidi. A* **28,** 683 (1974).
21. J. Smit and H. P. J. Wijn, *in* "Ferrites," p. 156. John Wiley and Sons, New York, 1959.
22. C. Barriga, V. Barron, R. Gancedo, M. Gracia, J. Morales, J. L. Tirado, and J. Torrent, *J. Solid State Chem.* **77,** 132 (1988).
23. P. D. Battle, T. C. Gibb, A. J. Heriod, S. H. Kim, and P. H. Munns, *J. Mater. Chem.* **5,** 865 (1995).
24. J. B. Goodenough, "Magnetism and the Chemical Bond," John Wiley and Sons, New York, London, 1963.
25. J. N. Reimers, J. R. Dahn, J. E. Greedan, C. V. Stager, G. Liu, I. Davidson, and U. von Sacken, *J. Solid State Chem.* **102,** 542 (1993).
26. A. Hirano, R. Kanno, Y. Kawamoto, Y. Takeda, K. Yamaura, M. Takano K. Ohyama, M. Ohashi, and Y. Yamaguchi, *Solid State Ionics* **78,** 123 (1995).
27. K. Yamaura, M. Takano, A. Hirano, and R. Kanno, *J. Solid State Chem.* **127,** 109 (1990).